PAPER

T–p phase diagrams and the barocaloric effect in materials with successive phase transitions

IOP Publishing Journal of Physics D: Applied Physics

J. Phys. D: Appl. Phys. **50** (2017) 384002 (10pp) https://doi.org/10.1088/1361-6463/aa8025

T–p phase diagrams and the barocaloric effect in materials with successive phase transitions

M V Gorev[1,2], E V Bogdanov[1,3] and I N Flerov[1,2]

[1] Kirensky Institute of Physics, Siberian Branch RAS, 660036 Krasnoyarsk, Russia
[2] Institute of Engineering Physics and Radioelectronics, Siberian Federal University, 660074 Krasnoyarsk, Russia
[3] Institute of Engineering Systems and Energy, Krasnoyarsk State Agrarian University, 660049 Krasnoyarsk, Russia

E-mail: gorev@iph.krasn.ru

Received 9 May 2017, revised 9 July 2017
Accepted for publication 17 July 2017
Published 30 August 2017

Abstract

An analysis of the extensive and intensive barocaloric effect (BCE) at successive structural phase transitions in some complex fluorides and oxyfluorides was performed. The high sensitivity of these compounds to a change in the chemical pressure allows one to vary the succession and parameters of the transformations (temperature, entropy, baric coefficient) over a wide range and obtain optimal values of the BCE. A comparison of different types of schematic *T–p* phase diagrams with the complicated $T(p)$ dependences observed experimentally shows that in some ranges of temperature and pressure the BCE in compounds undergoing successive transformations can be increased due to a summation of caloric effects associated with distinct phase transitions. The maximum values of the extensive and intensive BCE in complex fluorides and oxyfluorides can be realized at rather low pressure (0.1–0.3 GPa). In a narrow temperature range around the triple points conversion from conventional BCE to inverse BCE is observed, which is followed by a gigantic change of both $|\Delta S_{BCE}|$ and $|\Delta T_{AD}|$.

Keywords: barocaloric effect, phase transition, phase diagram, entropy

(Some figures may appear in colour only in the online journal)

1. Introduction

In recent years, caloric effects (CE) near phase transitions in solids of different physical origins have attract growing interest from investigators, as evidenced by the increasing number of relevant publications. Increased attention to this phenomenon is caused by two factors. The first is due to the possibility of obtaining information about a direct relationship between such fundamental values as entropy, temperature, order parameter, structural disorder and sensitivity to external fields (electric, magnetic, mechanical stress and hydrostatic pressure) [1–5]. The second is associated with the actual problem of searching for high-performance solid refrigerants for designing alternative refrigeration cycles which are competitive with to the traditional vapor compression cycles [6–9].

CE in solids can be initiated by change in the external field leading to a change in entropy, ΔS_{CE}, at constant temperature (extensive CE) or in temperature, ΔT_{AD}, at constant entropy (intensive CE). In accordance with the origin of both field and conjugated order parameters (polarization, magnetization, linear and volume strain), electrocaloric (ECE), magnetocaloric (MCE), elastocaloric (ElCE) and baroclaoric (BCE) effects are known [1]. The two first effects have been studied rather intensively for a long time and as a result a series of outstanding reviews devoted to MCE [10–15] and ECE [16, 17] have been published.

MCE, ElCE and BCE, studied for the first time in the 19th century [18, 19], have been rather actively explored in the past two decades [20–23] due to their significant advantage compared to other CE. Indeed, these effects are universal because

phase transitions in materials of different natures are very often accompanied by linear or volume strain of the crystal lattice which can be considered as one of the order parameters. The relationship between, on the one hand, extensive ΔS_{BCE} and intensive ΔT_{AD} BCE and, on the other, volume strain can be derived from Maxwell's equations and presented as follows [1]:

$$\Delta S_{BCE} = \int_0^p \left(\frac{\partial V}{\partial T}\right)_p \mathrm{d}p,$$
$$\Delta T_{AD} = -\int_0^p \frac{T}{C_p}\left(\frac{\partial V}{\partial T}\right)_p \mathrm{d}p. \quad (1)$$

CE of any nature are studied mainly in solids undergoing only one phase transition. Very often the most remarkable ΔS_{CE} and ΔT_{AD} have been observed in materials undergoing phase transitions of magnetic origin [1, 10, 24]. However, recent studies of some ferroelectrics, ferroelastics and superelastic magnetic alloys have shown that intensive and extensive BCE and ElCE can be considered as competitive effects in relation to MCE [3, 24–26].

In recent years, attention has also been given to paired and multicaloric effects involving BCE or ElCE in combination with MCE and/or ECE at the same transformation [2, 27–31]. It was shown that by using two different fields one can increase the total ΔS_{CE} and ΔT_{AD} values.

The effect of successive phase transitions on caloric efficiency has been less well explored. There are only a few papers devoted to the study of ECE near multiphases points in order to increase the entropy change [32–35]. However, as will be shown below, the phase transition entropy is only one of the two important parameters which characterize the caloric efficiency of materials. Equally important is the susceptibility of the phase transition temperature to the external field.

The present paper aims to look at the compromise between the phase transition entropy and baric coefficient at successive structural transformations and around triple points, i.e. between extensive and intensive BCE. Suitable objects for studying this interesting and intriguing question are complex fluorides and oxyfluorides containing anionic polyhedral species in their structure and demonstrating a great variety of successive structural transformations in one material at atmospheric or high pressure [36, 37]. It is worth mentioning as an outstanding example the crystal $(NH_4)_3ZrF_7$ undergoing six phase transitions in a rather narrow temperature range from 240 K to 290 K [38]. We discuss the behavior of both extensive and intensive BCE in related complex fluorides and oxyfluorides undergoing very often successive phase transitions of ferroelastic origin. Most attention is paid to analysis of the dependence of the barocaloric efficiency on the relative position of the phase boundaries and triple points in the *T*–*p* phase diagrams which are influenced by the chemical pressure.

2. Structural disorder and *T*–*p* phase diagrams in complex fluorides and oxyfluorides

Many complex fluorides and oxyfluorides with octahedral or quasi-octahedral anionic groups in their structure are characterized by a high symmetry of the initial crystal phase [36, 37]. X-ray diffraction (XRD) and related modeling have revealed that this point is associated with dynamical disordering of different structural units: individual atoms and/or atomic groups. Very often these compounds undergo one or more successive structural transformations upon cooling associated with a change in the degree of structural disorder and accompanied by large entropy change ΔS typical for the order–disorder processes [36, 37, 39].

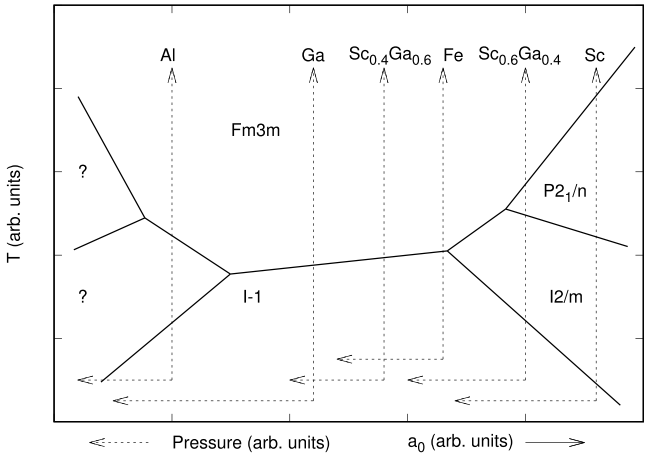

Figure 1. Generalized phase diagram temperature–pressure/parameter of the cubic unit cell, a_0, of the series of fluorides $(NH_4)_3Me^{3+}F_6$ and solid solutions. The *T*–*p* phase diagrams for the individual compounds are shown by dashed lines.

Equations (1) show that in order to realize noteworthy BCE the change in volume should also be large. This means that according to the Ehrenfest equation

$$\mathrm{d}T/\mathrm{d}p = T_0 V^{-1}(\partial \Delta V/\partial T)\Delta C_p^{-1} = T_0 \Delta\beta \Delta C_p^{-1} \quad (2)$$

and the Clausius–Clapeyron equation

$$\mathrm{d}T/\mathrm{d}p = \Delta V \Delta S^{-1} \quad (3)$$

for transformations of the second and first order, respectively, material considered as a potential refrigerant should demonstrate a high susceptibility to pressure. In equations (2) and (3), T_0 is the temperature of the phase transition and ΔV,ΔS, ΔC_p and $\Delta\beta$ are jumps at T_0 of volume, entropy, heat capacity and coefficient of the volume expansion, respectively.

Baric coefficients, $\mathrm{d}T/\mathrm{d}p$, for neighboring transformations in the same crystal of fluorides and oxyfluorides can be characterized by the same or different signs. This means that the BCE may be direct and/or inverse in the same material at different temperature and/or pressure. The *T*–*p* phase diagrams of some compounds under consideration also show triple points initiated by pressure at $p = p_{trp}$, which are associated with a splitting or merging of the phase boundaries with increase in pressure. So there is the possibility of changing the value and sign of BCE in the narrow temperature and pressure ranges around triple points.

Thus, it is obvious that susceptibility of temperature of the phase transition to external pressure $|\mathrm{d}T/\mathrm{d}p|$ and the value of the phase transition entropy ΔS are important criteria in the search for solid refrigerants with optimal barocaloric properties.

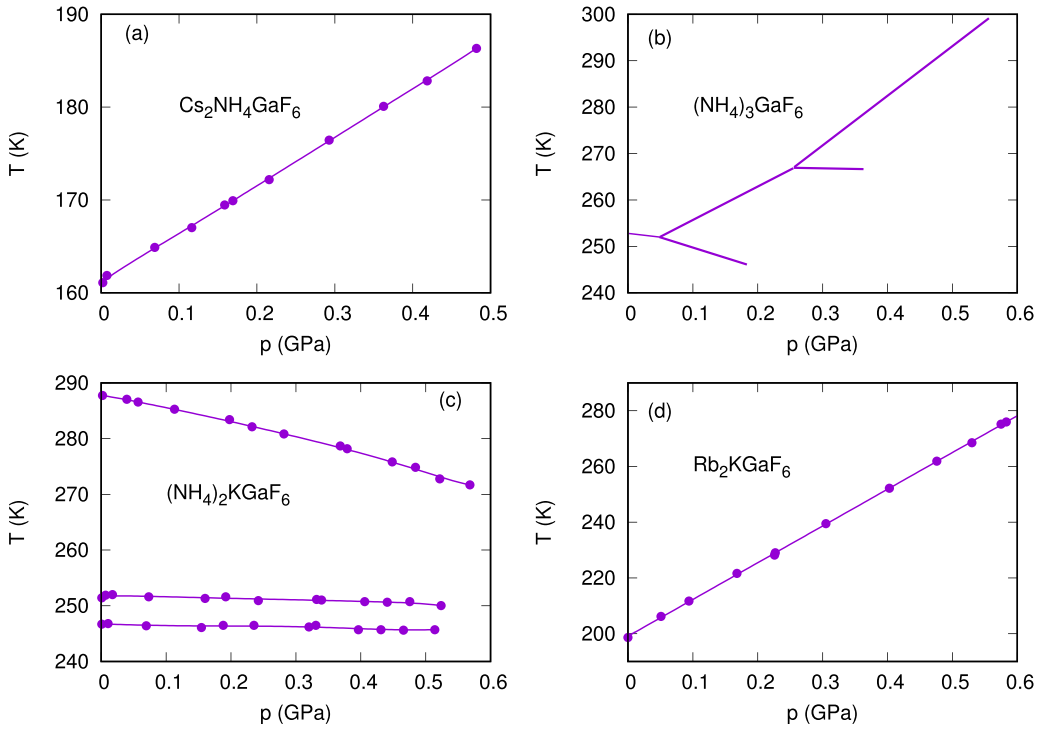

Figure 2. *T–p* phase diagrams of the fluorides $A_2A'GaF_6$ (A, A': Cs, Rb, NH_4, K).

Another attractive and important feature of complex fluorides and oxyfluorides is their ability to change chemical pressure in the crystal lattice using cationic–anionic substitution. Such an effective instrument allowed significant variation of the successions of structural transformations and their temperatures, the degree of structural disorder and associated entropy, the sign and value of the $(\partial V/\partial T)_p$ derivative and, as a result, dT/dp [36, 37]. One of the most visible examples proving this statement can be demonstrated using a generalized phase diagram temperature–pressure/parameter of the cubic unit cell, a_0, of the series of fluorides $(NH_4)_3Me^{3+}F_6$ (Me^{3+}: Al, Ga, Fe, Sc) (figure 1) and some of their solid solutions [37, 40, 41].

One can see that the size of the central atom in the $[MeF_6]$ polyhedron plays a significant role in the formation of different successions of the structural phase transitions between the initial $Fm\bar{3}m$ and final $I\bar{1}$ phases characterized by the different values and signs of the baric coefficients. However, a change in the total entropy associated with such a symmetry change is the same and very large in all the compounds and solid solutions: $\sum \Delta S = R \ln 16$ [40, 41].

Figure 2 shows the *T–p* phase diagrams of the fluorides $A_2A'GaF_6$ (A, A': Cs, Rb, NH_4, K) designated by different combinations of monovalent cations and having the same cubic symmetry of the initial phase, $Fm\bar{3}m$ [40, 42, 43]. In such a case, besides different mutual disposition, of the phase boundaries, there is a different degree of disordering of a cubic phase as demonstrated by rather distinct values of the phase transition entropies: $\sum \Delta S = R \ln 6$ in $(NH_4)_2KGaF_6$ [43] and $\Delta S = R \ln 16$ in $(NH_4)_3GaF_6$ [40].

The strong effect of cationic substitution on the structure of fluorides and oxyfluorides has been explained in terms of the bond stresses between different structural units [37]. By changing these parameters one can significantly decrease the structural disorder in a cubic phase $Fm\bar{3}m$ and stabilize it down to helium temperatures.

3. Barocaloric properties at successive phase transitions

To determine barocaloric properties, we used an approach similar to that suggested in [21–23, 44] and based on the analysis of experimental data on heat capacity at $p = 0$, the *T–p* phase diagram as well as the effect of pressure on the value and behavior of the phase transition entropy ΔS.

Because the ferroelastic compounds under consideration are characterized by strong ionic bonds, it was possible to confidently assume that the rather low pressure ($p < 1$ GPa) usually used in experiments with BCE does not substantially affect the behavior of the lattice heat capacity $C_{L(T)}$ or the lattice entropy $S_{L(T)}$. Differential thermal analysis (DTA) under pressure performed on the series of complex fluorides and oxyfluorides revealed that, on the one hand, the phase transition temperatures are shifted to varying degrees, for example $dT_0/dp > 0$ (figure 3(a)), and, on the other, entropy of the phase transitions, ΔS_0, remains almost unchanged with increase in pressure [44–46]. The latter point means that pressure did not significantly change the degree of disorder of the structural units in the initial and distorted phases. Information on the behavior of the lattice $S_{L(T)}$ and anomalous $\Delta S(T)$ entropies was obtained by integration of the $C_{L(T)}/T$ and $\Delta C_p(T)/T$ dependences, respectively. The total entropy for $p > 0$ as a function of temperature and pressure was determined by summation of $S_{L(T)}$ and $\Delta S(T, p)$ (figure 3(b)). The latter value was determined at $p = 0$ and shifted along the temperature scale in accordance with baric coefficient dT_0/dp

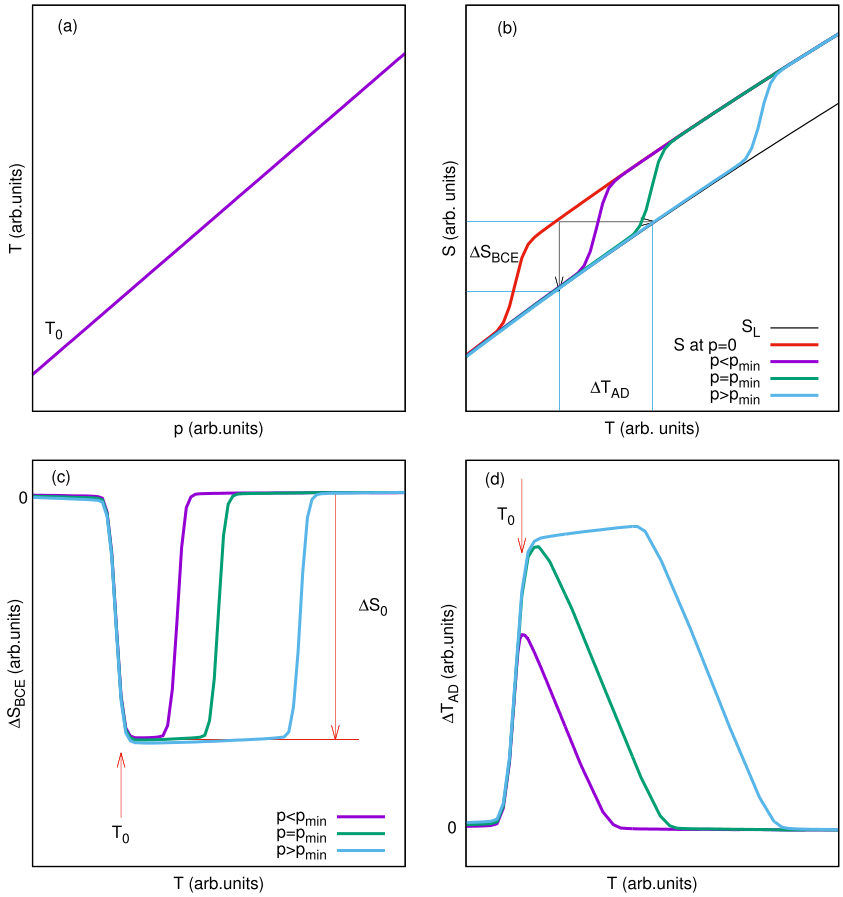

Figure 3. Schematic presentation of the T–p phase diagram for a single phase transition (a). Temperature dependences of the total entropy (b), extensive BCE (c) and intensive BCE (d) at different pressures.

$$S(T,p) = S_{\mathrm{L(T)}} + \Delta S(T + (\mathrm{d}T_0/p)\,p). \tag{4}$$

Because ΔS_{BCE} and ΔT_{AD} correspond to conditions $T = \mathrm{const}$ and $S = \mathrm{const}$, respectively, analysis of the temperature and pressure dependences of the total entropy allows one to determine $\Delta S_{\mathrm{BCE}}(T,p) = S(T,p \neq 0) - S(T,p = 0)$. The maximum extensive BCE ΔS_{BCE} as well as any other extensive CE ΔS_{CE} is limited by entropy of the phase transitions ΔS [47]. The ΔT_{AD} value was defined from equation $S(T,p) = S(T + \Delta T_{\mathrm{AD}}, 0)$.

Rather often the T–p phase diagrams of materials under consideration consist of linear or/and nonlinear phase boundaries and show a splitting/merging in one or several triple points with close values of pressure and temperature. So to start it makes sense to analyze peculiarities of the temperature behavior of BCE depending on pressure in connection with some simple schematic phase diagrams (figures 3–5), which are qualitatively similar to some diagrams observed experimentally (figures 1 and 2). The ratio between entropies of the successive phase transitions was chosen arbitrarily. We also take into account an assumption from above based on the experimental data showing that the entropy of the transformations is weakly dependent on pressure [44–46].

In the case of a single phase transition (figure 3(a)) with the positive baric coefficient, ΔS_{BCE} quickly reaches the maximum value (figure 3(b)) equal to the phase transition entropy ΔS_0, i.e. at rather low pressure. Maximum value of the intensive BCE, $\Delta T_{\mathrm{AD}}^{\max} = -T\Delta S_{\mathrm{BCE}}/C_{\mathrm{L}}$, is observed at $p > p_{\min}$ (figure 3(c)) where $p_{\min}$ is minimal pressure which produces the maximum values of BCE.

$$\Delta T_{\mathrm{AD}}^{\max} = p_{\min}\mathrm{d}T_0/\mathrm{d}p,$$
$$p_{\min} = (T\Delta S)/(C_p\mathrm{d}T_0/\mathrm{d}p). \tag{5}$$

Both extensive and intensive BCE exist in the range of $T_0(p = 0) - T_0(p)$. In accordance with (1), the maximum value of the intensive BCE $\Delta T_{\mathrm{AD}}^{\max}$ is also limited by the ΔS value but depends on the $(\partial S_{\mathrm{L}}/\partial T)_p$ derivative, i.e. on the temperature region where phase transition takes place. At $\mathrm{d}T_0/\mathrm{d}p < 0$, the sign of the both extensive and intensive BCE in figures 3(b) and (c) will also be changed to the opposite sign.

Two variants of the T–p phase diagrams are possible in materials undergoing two successive phase transitions: with the same (figure 4(a)) and different (figure 4(d)) values of $\mathrm{d}T_1/\mathrm{d}p$ and $\mathrm{d}T_2/\mathrm{d}p$ characterized by the same sign. In this case, BCE rises in the temperature range from $T_1(p = 0)$ to $T_2(p > p*)$, where $p* = (T_1 - T_2)/(\mathrm{d}T_2/\mathrm{d}p)$, and ΔS_{BCE} can reach a value equal to $\Delta S_1 + \Delta S_2$ and remain constant at further increase in pressure (figure 4(b)). However, the intensive BCE achieves $\Delta T_{\mathrm{AD}}^{\max}$ at higher pressure (figure 4(c)).

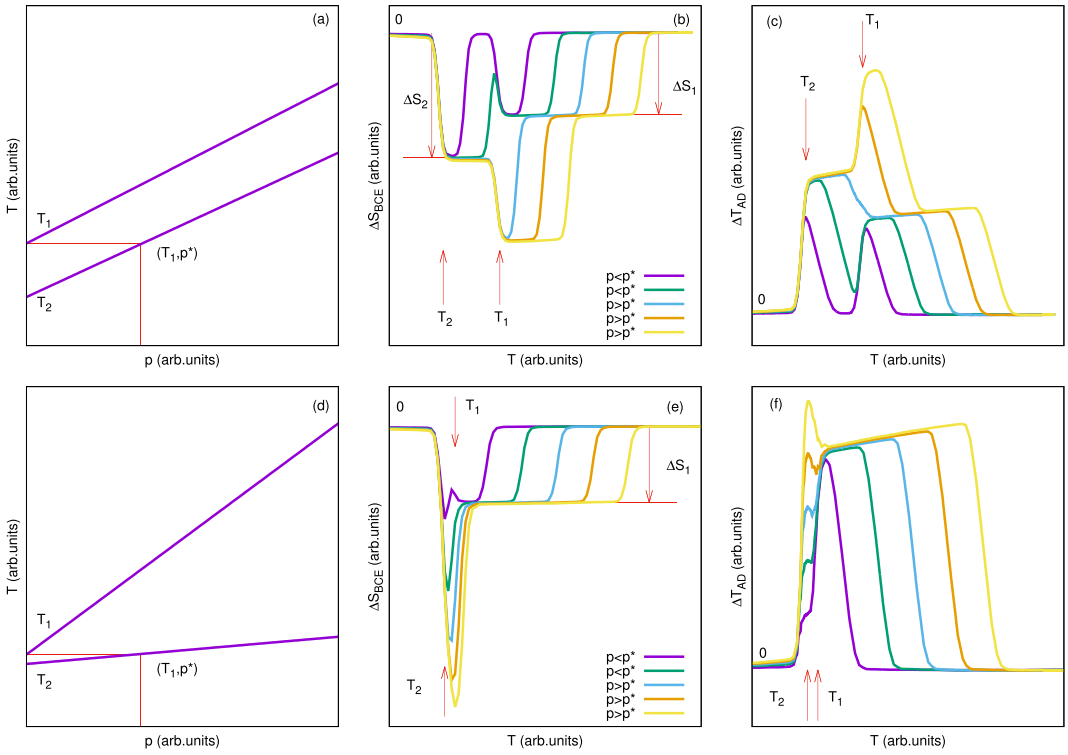

Figure 4. Schematic presentation of the *T*–*p* phase diagrams for successive phase transitions ((a), (d)) and related temperature dependences of extensive ((b), (e)) and intensive ((c), (f)) BCE at different pressures.

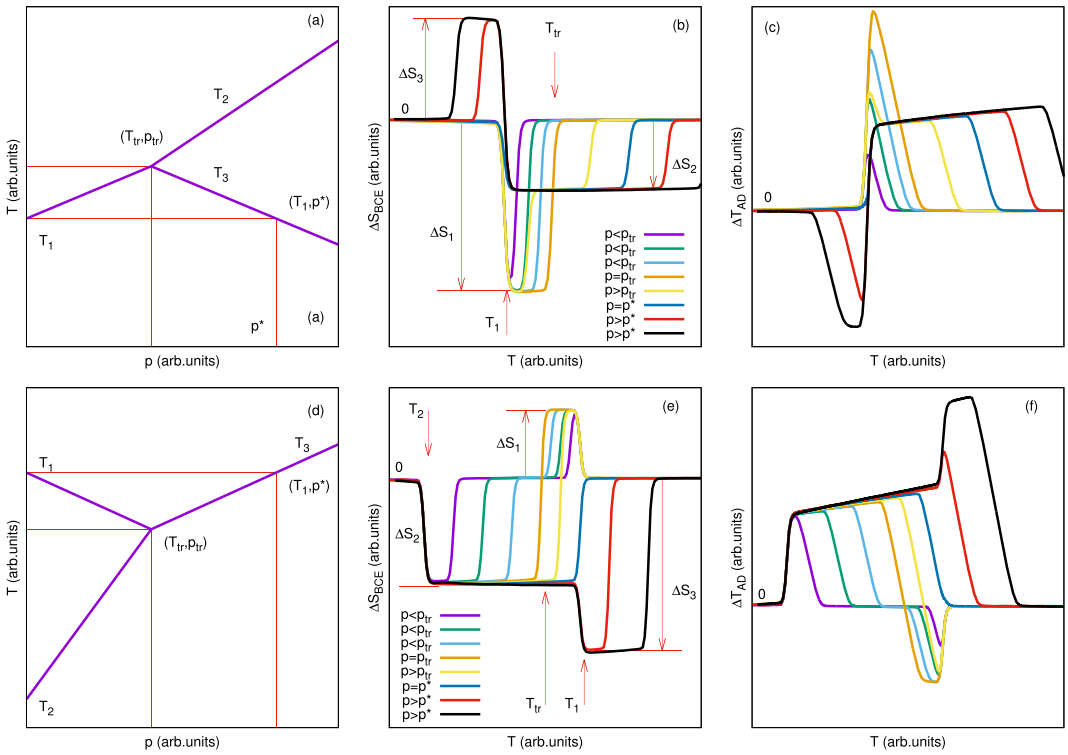

Figure 5. Schematic presentation of the *T*–*p* phase diagrams with triple points ((a), (d)) and related temperature dependences of extensive ((b), (e)) and intensive ((c), (f)) BCE at different pressures.

The presence of one triple point on the *T*–*p* phase diagram can be associated with two variants of the BCE behavior depending on several parameters (figure 5). In the first case (figure 5(a)), three characteristic pressure regions exist. At $T_1(p=0) < T < T_{\mathrm{trp}}$, increase in pressure from $p=0$ to $p=p_{\mathrm{trp}}$ is accompanied by an increase of extensive and intensive effects up to maximum values ΔS_1 and $\Delta T_{\mathrm{AD}} = -T\Delta S_1/C_{\mathrm{L}}$, when $p_{\mathrm{min1}} < p_{\mathrm{trp}}$. At pressure just

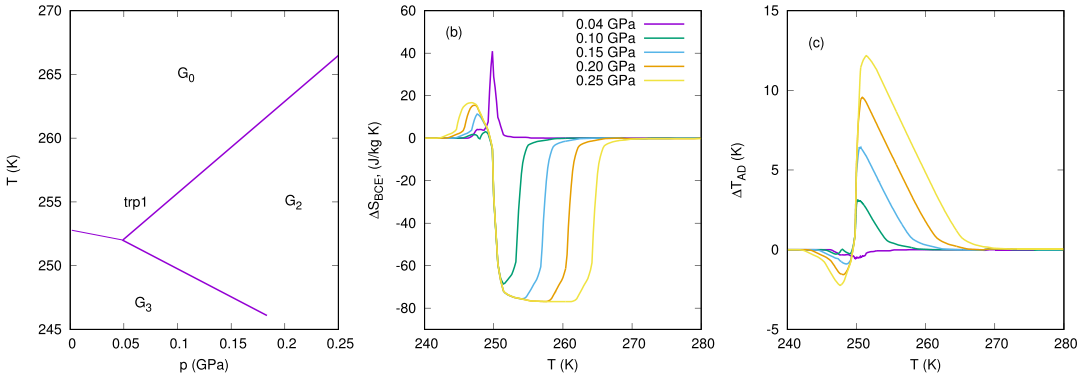

Figure 6. *T*–*p* phase diagram of $(NH_4)_3GaF_6$ (a) and related temperature dependences of ΔS_{BCE} (b) and ΔT_{AD} (c) at different pressures.

above p_{trp}, the temperature region of BCE existence associated with ΔS_1 narrows; however, BCE associated with ΔS_2 appears (figures 5(b) and (c)). At $p > p*$, an inverse BCE appears below $T_1(p = 0)$ in accordance with $dT_2/dp < 0$, which very quickly achieves the maximum values of ΔS_{BCE} and ΔT_{AD}. Caloric effects at this pressure in the region of $T < T_1(p = 0)$ and $T > T_1(p = 0)$ depend on parameters of the phase transitions realized at $p > p_{trp}$ and at higher pressure, $p > p_{trp} + p_{min2}$, $p > p_{trp} + p_{min3}$, they reach maximum values.

In the situation presented in figures 5(e) and (f) extensive and intensive BCE associated with the distinct phase transitions at $p < p_{trp}$ are observed in the two temperature regions below $T_1(p = 0)$ and above $T_2(p = 0)$. They expand under pressure up to the triple point, and can achieve maximum values when p_{trp} is lower than p_{min1} and p_{min2}. At $p > p_{trp}$, the temperature region with conventional BCE continues to expand. The region of existence of inverse BCE narrows and disappears at $p = p*$. Above $T_1(p = 0)$, further increase in pressure leads to the appearance of BCE with the following values: $\Delta S_{BCE} = \Delta S_1 + \Delta S_2$ and $\Delta T_{AD} = -T\Delta S_{BCE}/C_L$.

The schematic phase diagrams considered above do not demonstrate all the possible variants of the dependences $T(p)$. However, the analysis is very important and informative because it allows one:

(i) to see the qualitative behavior of extensive and intensive BCE in conventional and inverse variants at successive structural transformations;
(ii) to evaluate p_{min} only on the basis of data on heat capacity and thermal expansion giving information on T_i, C_p, ΔC_p, ΔS_i, ΔV_i, $\Delta\beta$ and dT_i/dp calculated using the Ehrenfest and Clausius–Clapeyron equations;
(iii) to carry out preliminary evaluations of the range of the p and T parameters associated with the most pronounced extensive and intensive BCE;
(iv) to reveal that both dependences $\Delta S_{BCE}(T)$ and $\Delta T_{AD}(T)$ have a plateau which is very important peculiarity of BCE compared with ECE and MCE, which in many cases look like smeared peaks.

It is very interesting to consider a change of the *T*–*p* phase diagrams and the development of BCE in some real fluoride and oxyfluoride crystals depending on chemical and hydrostatic pressure.

The generalized *T*–*p* phase diagram of fluorides $(NH_4)_3Me^{3+}F_6$ (figure 1) [40] clearly demonstrates a significant effect of chemical pressure on temperature of the phase transition from the initial cubic phase $Fm\bar{3}m$ and the related baric coefficient dT/dp. The part of this diagram for $(NH_4)_3GaF_6$ shown in figure 6 is similar to the diagram analyzed in figure 5(a), at least in the pressure range up to the first triple point.

In accordance with the discussion above and the low value of the baric coefficient $dT_0/dp = -12$ K GPa^{-1}, it is obvious that a direct transformation $Fm\bar{3}m \leftrightarrow I\bar{3}a$ in this compound could not be associated with large BCE in spite of a significant change in the entropy $\Delta S_0 = 23$ J mol^{-1} K^{-1}. Indeed, figures 6(b) and (c) show that at $p = 0.04$ GPa there is an inverse BCE characterized by very small values of both extensive and intensive effects ΔS_{BCE} and ΔT_{AD}. However, due to the low pressure of the triple point 1, $p_{trp1} \approx 0.045$ GPa, at $p = 0.1$ GPa $> p_{trp1}$ a succession of two transformations $G_0 \leftrightarrow G_2 \leftrightarrow G_3$ appeared, one of which, $G_0 \leftrightarrow G_2$, is accompanied by a large positive value of $dT/dp = 73$ K GPa^{-1} and a significant change in the entropy $\Delta S = 18$ J mol^{-1} K^{-1} [40]. The temperature behavior of ΔS_{BCE} and ΔT_{AD} at different pressures in $(NH_4)_3GaF_6$ is qualitatively similar to that demonstrated in the schematic phase diagram (figures 6(b) and (c)). Indeed, a maximum value of the extensive BCE, $\Delta S^{max}_{BCE} = -96$ J mol^{-1} K^{-1}, associated with the phase transition $G_0 \leftrightarrow G_2$ can be achieved at very low pressure $p = 0.15$ GPa, whereas in accordance with equation (5) $\Delta T^{max}_{AD} = 14.5$ K can be realized at about $p_{min} + p_{trp1} = 0.25$ GPa.

One more interesting example of the development of the BCE at successive structural transformations is connected with $(NH_4)_3ScF_6$ characterized by a larger unit cell volume than $(NH_4)_3GaF_6$ [40]. Figure 7 demonstrates a similar behavior of both types of BCE compared with a schematic presentation in figures 5(e) and (f). We do not consider BCE at the phase transition $G_2 \leftrightarrow G_3$ because of a very small value of $\Delta S = 0.7$ J mol^{-1} K^{-1}. The 'wings' of anomalous peaks associated with the inverse and conventional effects at $G_0 \leftrightarrow G_1$ and $G_1 \leftrightarrow G_2$ transformations, respectively, are approaching each other with increasing pressure. At $p \geqslant p_{trp1} = 0.52$ GPa, there is a smooth transition between the two types of BCE accompanied by a change of ΔS^{max}_{BCE} from $+56$ to -28 J mol^{-1} K^{-1} and ΔT^{max}_{AD} from -8 to $+5$ K. In accordance with the analysis of

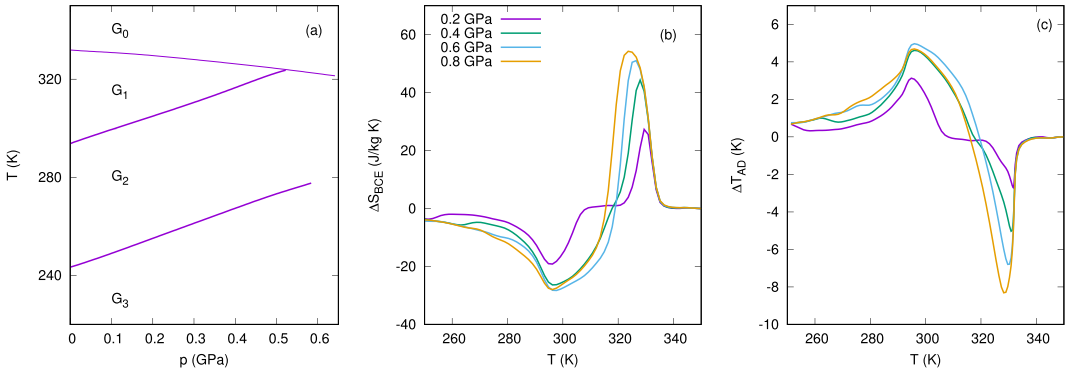

Figure 7. *T*–*p* phase diagram of $(NH_4)_3ScF_6$ (a) and related temperature dependences of ΔS_{BCE} (b) and ΔT_{AD} (c) at different pressures.

the similar situation in figures 5(d)–(f), the maximum value of the inverse BCE at the direct transformation $G_0 \leftrightarrow G_2$ in $(NH_4)_3ScF_6$ can be achieved at rather high pressure, $p > p* = 2.3$ GPa. The results of study of the solid solutions $(NH_4)_3Ga_{1-x}Sc_xF_6$ allow one to assume that this situation can be improved in compounds with $x \approx 0.6$, characterized by a narrow temperature range of G_1 phase existence ($\sim$12 K) and lower value of $p* \approx 1$ GPa [48].

Figure 2 shows that a change in chemical pressure initiated by a cationic substitution in fluorides $A_2A'GaF_6$ strongly affects all the parameters of the phase transitions: temperature, entropy and baric coefficient. Besides $(NH_4)_3GaF_6$, successive transformations were found only in $(NH_4)_2KGaF_6$ [43]. However, due to rather the low entropy and baric coefficient, none of the three transitions is of interest regarding BCE. The parameters of conventional BCE in Rb_2KGaF_6 and $Cs_2NH_4GaF_6$ associated with one phase transition are close to each other and are worth mentioning: $\Delta S^{max}_{BCE} = -36$ J kg^{-1} K^{-1}, $\Delta T^{max}_{AD} = 12$ K, $p_{min} = 0.1$ GPa (Rb_2K) and $\Delta S^{max}_{BCE} = -34$ J kg^{-1} K^{-1}, $\Delta T^{max}_{AD} = 13$ K, $p_{min} = 0.24$ GPa (Cs_2NH_4).

Some oxyfluorides with polar anionic polyhedra in the structure are also characterized by a high degree of disorder in the initial phase and the high susceptibility to pressure. As a result many of them demonstrate *T*–*p* phase diagrams rich in triple points and high pressure phases [36, 37]. These properties make fluoro-oxygen compounds very promising for the investigation of their barocaloric efficiency. Analysis of BCE in compounds with the cryolite structure (space group $Fm\bar{3}m$) undergoing one phase transition has shown an opportunity to realize very large values of $\Delta S^{max}_{BCE} \approx$ (35–47) J kg^{-1} K^{-1} and $\Delta T^{max}_{AD} \approx (16-19)$ K at rather low pressure p_{min} [3, 22, 44, 46]. Here, we will discuss BCE in oxyfluorides with the same central atom in anion polyhedra coordinated in different ways: $(NH_4)_2NbOF_5$, $(NH_4)_3Nb(O_2)_2F_4$, $(NH_4)_3NbOF_6$.

$(NH_4)_2NbOF_5$ with a six-coordinated polyhedron $[NbOF_5]^{3-}$ undergoes upon cooling a succession of the two structural phase transitions $Cmc2_1(T_1) \leftrightarrow C2(T_2) \leftrightarrow Ia$ accompanied by gigantic total entropy change $\sum \Delta S = (21.6 + 16.6)$ J mol^{-1} K^{-1} $\approx R \ln 12 + R \ln 8$ due to the orientational ordering of both distorted $[NbOF_5]^{2-}$ octahedra and ammonium tetrahedra [48]. The *T*–*p* phase diagram of this oxyfluoride (figure 8(a)) is a variant of the schematic diagram discussed above (figure 4(a)), when hydrostatic pressure leads to a linear change in the transition temperatures of two transformations with almost the same baric coefficients: $dT_1/dp = -45.4$ K GPa^{-1} and $dT_2/dp = -45.2$ K GPa^{-1}.

In accordance with the negative sign of dT_i/dp the BCE at both transformations in $(NH_4)_2NbOF_5$ are inverse ($\Delta T_{AD} < 0$, $\Delta S_{BCE} > 0$) (figures 8(b) and (c)) [48]. It is obvious that the maximum possible magnitude of the extensive BCE is equal to the value of the entropy change associated with both phase transitions, $\Delta S^{max}_{BCE} = 155$ J kg^{-1} K^{-1}. However, this entropy is divided between two transformations, and until $T_2(p = 0) < T_1(p) = T_1(p = 0) + p \cdot dT_1/dp$ two separate overlapped peaks of ΔS_{BCE} are observed. At $p > 0.85$ GPa, $T_2(p = 0) > T_1(p)$ and an increase in ΔS_{BCE} is observed. However, rather large pressure is required to achieve ΔS^{max}_{BCE} and ΔT^{max}_{AD}. The temperature behavior of both types of BCE is qualitatively similar to that presented in the schematic diagram (figures 4(b) and (c)). A smearing of the $\Delta S_{BCE}(T)$ and $\Delta T_{AD}(T)$ peaks in $(NH_4)_2NbOF_5$ can be explained by the existence of the anomalous contribution to the entropy associated with a change of the order parameters in a wide temperature range.

Analysis of ElCE in $(NH_4)_2NbOF_5$ has shown very interesting results associated with a strong anisotropy in the susceptibility to uniaxial pressure [48]. As a result conventional ElCE was observed along *a* and *b* axes at T_1 and T_2, respectively. The main contribution into the inverse BCE is associated with the inverse ElCE along the *c* axis.

Another niobate, $(NH_4)_3Nb(O_2)_2F_4$, has an eight-coordinated anion polyhedron and is characterized at room temperature by the cubic structure (space group $Fm\bar{3}m$) with disordered fluoro-oxygen polyhedra and ammonium tetrahedra [49]. The total entropy change associated with the two phase transitions at close temperatures, $T_1 = 193$ K and $T_2 = 186$ K, is characteristic for the order–disorder processes $\sum \Delta S = 23$ J mol^{-1} K^{-1} $\approx R \ln 16$ [49]. However, the pressure dependence of temperatures of the both transformations is characterized by strong nonlinearity described by the equations $T_1 = 193 - 57.4p + 160p^2$ and $T_2 = 186 - 44.4p + 228p^2$ [49] (figure 9(a)). Thus, it is not surprising that extensive BCE increases rather quickly with increase in pressure ($\Delta S_{BCE} = 42$ J kg^{-1} K^{-1} at $p = 0.2$ GPa) but exists in very narrow range of the temperature (figure 9(b)).

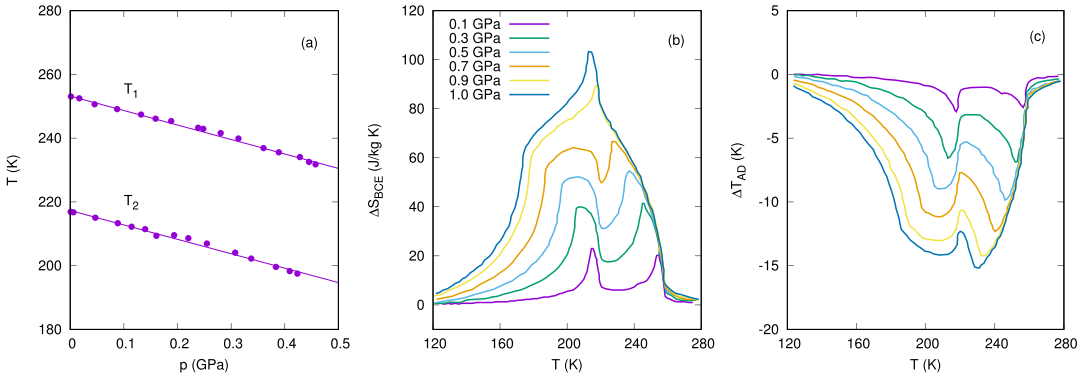

Figure 8. T–p phase diagram of $(NH_4)_2NbOF_5$ (a) and related temperature dependences of ΔS_{BCE} (b) and ΔT_{AD} (c) at different pressures.

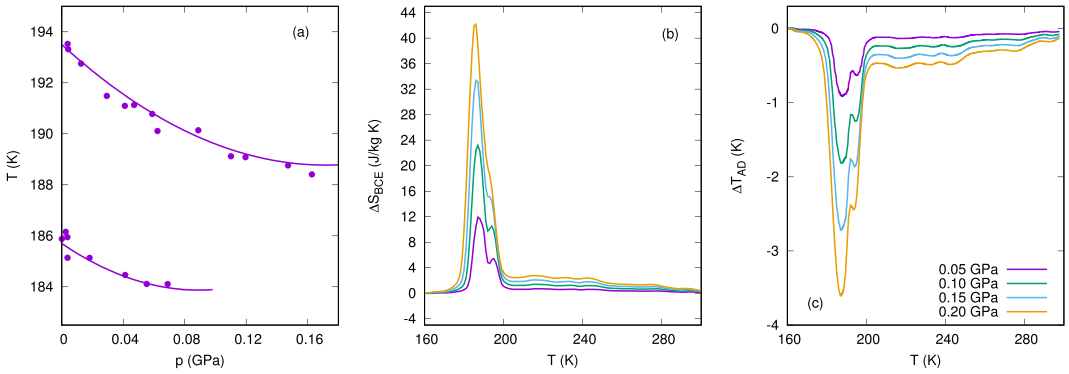

Figure 9. T–p phase diagram of $(NH_4)_3Nb(O_2)_2F_4$ (a) and related temperature dependences of ΔS_{BCE} (b) and ΔT_{AD} (c) at different pressures.

Low values of dT_i/dp are also the reason for small intensive BCE (figure 9(c)).

The substitution of eight-coordinated polyhedra by seven-coordinated ones did not change the cubic structure $Fm\bar{3}m$ and resulted in the entropy increase caused by successive phase transitions, from $\sum \Delta S_i \approx R \ln 16$ in $(NH_4)_3Nb(O_2)_2F_4$ to $\sum \Delta S_i \approx R \ln 96$ in $(NH_4)_3NbOF_6$ [50]. The T–p phase diagram of $(NH_4)_3NbOF_6$ is similar to the diagram presented in figure 4(d) and associated with the successive phase transitions characterized by a strong difference in the baric coefficients. The analysis has shown that maximum values of the extensive and intensive BCE near some transformations and around triple points are worthy of attention—$\Delta S_{BCE}^{max} = -30$ to 100 J mol^{-1} K^{-1} and $\Delta T_{AD}^{max} = 6$ to -15 K—and can be achieved at pressure 0.1–1.25 GPa.

A comparative analysis of caloric efficiency in different types of ferroics has shown that BCE in some ferroelastic fluorides and oxyfluorides undergoing one phase transition is comparable with the greatest values of MCE, ECE and BCE observed recently in other materials [6, 17, 24]. The results obtained in the present paper show that further increase of the BCE can be realized in compounds undergoing successive transformations. In such a case in some ranges of temperature and pressure the BCE can reach values equivalent to the sum of caloric effects associated with distinct phase transitions.

4. Conclusions

We performed a pioneering analysis of the extensive and intensive BCE at successive structural phase transitions in some complex fluorides and oxyfluorides which are very sensitive to a change of chemical pressure. Different types of T–p phase diagrams including the triple points are considered in connection with the complicated dependences $T(p)$ observed experimentally. The analyzed diagrams do not cover all possible variants of the phase transition–temperature behavior under pressure. However, they show which parameters of the phase transitions and phase diagrams should be taken into consideration when analyzing BCE. A very important point is that, contrary to some ferroelectric crystals [25, 26, 51], rather low hydrostatic pressure has practically no effect on an entropy of ferroelastic transformations, therefore the behavior of extensive and intensive BCE is not changed with increase in pressure. In the case of successive phase transitions at close temperatures there is a possibility of realizing extensive BCE as the sum of ΔS of two transformations. A comparison of BCE with MCE and ECE has shown that ferroelastics undergoing single or successive phase transitions are competitive solid refrigerants [6, 17, 24]. Moreover, at pressures above p_{min} both dependences $\Delta S_{BCE}(T,p)$ and $\Delta T_{AD}(T,p)$ show a plateau which is a very important peculiarity of BCE.

Acknowledgments

The reported study was funded by Russian Foundation for Basic Research, Government of Krasnoyarsk Territory, Krasnoyarsk Region Science and Technology Support Fund to the research project no. 17-42-240076 p-a.

References

[1] Tishin A M and Spichkin Y I 2003 *The Magnetocaloric Effect and its Applications* (Bristol: Institute of Physics Publishing)
[2] Lisenkov S, Mani B K, Chang C-M, Almand J and Ponomareva I 2013 Multicaloric effect in ferroelectric $PbTiO_3$ from first principles *Phys. Rev.* B **87** 224101
[3] Flerov I N, Gorev M V, Tressaud A and Laptash N M 2011 Perovskite-like fluorides and oxyfluorides: phase transitions and caloric effects *Cryst. Rep.* **56** 9–17
[4] Flerov I N, Mikhaleva E A, Gorev M V and Kartashev A V 2015 Caloric and multicaloric effects in oxygen ferroics and multiferroics *Phys. Solid State* **57** 429–41
[5] de Oliveira N A, von Ranke P J and Troper A 2014 Magnetocaloric and barocaloric effects: theoretical description and trends *Int. J. Refrig.* **37** 237–48
[6] Mañosa L, Planes A and Acet M 2013 Advanced materials for solid-state refrigeration *J. Mater. Chem.* A **1** 4925–36
[7] Sinyavski Y V, Lugansky G E and Pashov N D 1992 Electrocaloric refrigeration: investigation of a mode, and prognosis of mass and efficiency index *Cryogenics* **32** 28
[8] Ožbolt M, Kitanovski A, Tušek J and Poredoš A 2014 Electrocaloric refrigeration: thermodynamics, state of the art and future perspectives *Int. J. Refrig.* **40** 174–88
[9] Lorusso G *et al* 2013 A dense metal-organic framework for enhanced magnetic refrigeration *Adv. Mater.* **25** 4653–6
[10] Gschneidner K A Jr, Pecharsky V K and Tsokol A O 2005 Recent developments in magnetocaloric materials *Rep. Prog. Phys.* **68** 1479
[11] Brück E 2008 *Handbook of Magnetic Materials* (Amsterdam: Elsevier) pp 235–91
[12] Franco V, Blázquez J S, Ingale B and Conde A 2012 The magnetocaloric effect and magnetic refrigeration near room temperature: materials and models *Ann. Rev. Mater. Res.* **42** 305
[13] Smith A, Bahl C R H, Bj R, Engelbrecht K, Nielsen K K and Pryds N 2012 Materials challenges for high performance magnetocaloric refrigeration devices *Adv. Energy Mater.* **2** 1288
[14] Wei Z, Chak-Tong A and You-Wie D 2013 Review of magnetocaloric effect in perovskite-type oxides *Chin. Phys.* B **22** 057501
[15] Planes A, Mañosa L and Acet M 2009 Magnetocaloric effect and its relation to shape-memory properties in ferromagnetic Heusler alloys *J. Phys.: Condens. Matter* **21** 233201
[16] Scott J F 2011 Electrocaloric materials *Ann. Rev. Mater. Res.* **41** 229
[17] Valant M 2012 Electrocaloric materials for future solid-state refrigeration technologies *Prog. Mater. Sci.* **57** 980
[18] Thomson W 1855 On the thermoelastic and thermomagnetic properties of matter. Part I *Quart. J. Math.* **1** 57
[19] Joule J P 1859 On some thermo-dynamic properties of solids *Phil. Trans.* **149** 91–131
[20] Müller K A, Fauth F, Fischer S, Koch M, Furrer A and Lacorre P 1998 Cooling by adiabatic pressure application in $Pr_{1-x}La_xNiO_3$ *Appl. Phys. Lett.* **73** 1056
[21] Strässle T, Furrer A, Hossain Z and Geibel Ch 2003 Magnetic cooling by the application of external pressure in rare-earth compounds *Phys. Rev.* B **67** 054407
[22] Gorev M V, Bogdanov E V, Flerov I N, Kocharova A G and Laptash N M 2010 Investigation of thermal expansion, phase diagrams, and barocaloric effect in the $(NH_4)_2WO_2F_4$ and $(NH_4)_2MoO_2F_4$ oxyfluorides *Phys. Solid State* **52** 167–75
[23] Mañosa L and Planes A 2017 Materials with giant mechanocaloric effects: cooling by strength *Adv. Mater.* **29** 1603607
[24] Moya X, Kar-Narayan S and Mathur N D 2014 Caloric materials near ferroic phase transitions *Nat. Mater.* **13** 439
[25] Lloveras P *et al* 2015 Giant barocaloric effects at low pressure in ferrielectric ammonium sulphate *Nat. Commun.* **6** 8801
[26] Mikhaleva E A, Flerov I N, Kartashev A V, Gorev M V, Bogdanov E V and Bondarev V S 2017 Thermal, dielectric and barocaloric properties of NH_4HSO_4 crystallized from an aqueous solution and the melt *Solid State Sci.* **67** 1–7
[27] Castillo-Villa P O 2011 Caloric effects induced by magnetic and mechanical fields in a $Ni_{50}Mn_{25-x}Ga_{25}Co_x$ magnetic shape memory alloy *Phys. Rev.* B **83** 174109
[28] Mikhaleva E A, Flerov I N, Gorev M V, Molokeev M S, Cherepakhin A V, Kartashev A V, Mikhashenok N V and Sablina K A 2012 Caloric characteristics of $PbTiO_3$ in the temperature range of the ferroelectric phase transition *Phys. Solid State* **54** 1832–40
[29] Mikhaleva E A, Flerov I N, Bondarev V S, Gorev M V, Vasiliev A D and Davydova T N 2012 Electrocaloric and barocaloric effects in some ferroelectric hydrosulfates and triglycinesulfate *Ferroelectrics* **430** 78–83
[30] Kartashev A V, Mikhaleva E A, Gorev M V, Bogdanov E V, Cherepakhin A V, Sablina K A, Mikhashonok N V, Flerov I N and Volkov N V 2013 Thermal properties, magneto- and baro-caloric effects in $La_{0.7}Pb_{0.3}MnO_3$ single crystal *J. Appl. Phys.* **113** 073901
[31] Starkov I A and Starkov A S 2014 On the thermodynamic foundations of solid-state cooler based on multiferroic materials *Int. J. Refrig.* **37** 249–56
[32] Xu Z, Fan Z, Liu X and Tan X 2017 Impact of phase transition sequence on the electrocaloric effect in $Pb(Nb,Zr,Sn,Ti)O_3$ ceramics *Appl. Phys. Lett.* **110** 082901
[33] Liu Z K, Li X and Zhang Q M 2012 Maximizing the number of coexisting phases near invariant critical points for giant electrocaloric and electromechanical responses in ferroelectrics *Appl. Phys. Lett.* **101** 082904
[34] Liu W and Ren X 2009 Large piezoelectric effect in Pb-free ceramics *Phys. Rev. Lett.* **103** 257602
[35] Luo Z, Zhang D, Liu Y, Zhou D, Yao Y, Liu Ch, Dkhil B, Ren X and Lou X 2014 Enhanced electrocaloric effect in lead-free $BaTi_{1-x}Sn_xO_3$ ceramics near room temperature *Appl. Phys. Lett.* **105** 102904
[36] Flerov I N, Gorev M V, Aleksandrov K S, Tressaud A, Grannec J and Couzi M 1998 Phase transitions in elpasolites (ordered perovskites) *Mater. Sci. Eng. R: Rep.* **24** 81–151
[37] Flerov I N, Gorev M V, Molokeev M S and Laptash N M 2016 *Photonic and Electronic Properties of Fluoride Materials* (*Progress in Fluorine Science Series*) ed A Tressaud and K Poeppelmeier (Amsterdam: Elsevier) pp 355–81
[38] Fokina V D, Gorev M V, Bogdanov E V, Pogoreltsev E I, Flerov I N and Laptash N M 2013 Thermal properties and phase transitions in $(NH_4)_3ZrF_7$ *J. Fluorine Chem.* **154**
[39] Flerov I N and Gorev M V 2001 Entropy and the mechanism of phase transitions in elpasolites *Phys. Solid State* **43** 127–36
[40] Gorev M V, Flerov I N, Tressaud A, Denu D, Zaitsev A I and Fokina V D 2002 A study of the phase diagrams of

$(NH_4)_3Ga_{1-x}Sc_xF_6$ ammonium cryolites *Phys. Solid State* **44** 1954–60

[41] Flerov I N, Gorev M V and Ushakova T V 1999 Calorimetric investigations of phase transitions in the cryolites $(NH_4)_3Ga_{1-x}Sc_xF_6$ ($x = 1.0, 0.1, 0$) *Phys. Solid State* **41** 468–73

[42] Gorev M V, Flerov I N, Tressaud A, Zaitsev A I and Durand E 2002 Heat capacity and $T - p$ phase diagram of $Cs_2NH_4GaF_6$ elpasolite *Solid State Sci.* **4** 15–8

[43] Flerov I N, Gorev M V, Afanas'ev M L and Ushakova T V 2001 Thermodynamic properties of $(NH_4)_2KGaF_6$ elpasolite *Phys. Solid State* **43** 2301–6

[44] Gorev M V, Flerov I N, Bogdanov E V, Voronov V N and Laptash N M 2010 Barocaloric effect near the structural phase transition in the Rb_2KTiOF_5 oxyfluoride *Phys. Solid State* **52** 377–83

[45] Pogoreltsev E I, Flerov I N, Kartashev A V, Bogdanov E V and Laptash N M 2014 Heat capacity, entropy, dielectric properties and T-p phase diagram of $(NH_4)_3TiF_7$ *J. Fluorine Chem.* **168** 247–50

[46] Flerov I N, Kartashev A V, Gorev M V, Bogdanov E V, Mel'nikova S V, Molokeev M S, Pogoreltsev E I and Laptash N M 2016 Thermal, structural, optical, dielectric and barocaloric properties at ferroelastic phase transition in trigonal $(NH_4)_2SnF_6$: a new look at the old compound *J. Fluorine Chem.* **183** 1–9

[47] Pirc R, Kutnjak Z, Blinc R and Zhang Q M 2011 Upper bounds on the electrocaloric effect in polar solids *Appl. Phys. Lett.* **98** 021909

[48] Gorev M, Bogdanov E, Flerov I and Laptash N 2010 Thermal expansion, phase diagrams and barocaloric effects in $(NH_4)_2NbOF_5$ *J. Phys.: Condens. Matter* **22** 185901

[49] Fokina V D, Bovina A F, Bogdanov E V, Pogorel'tsev E I, Laptash N M, Gorev M V and Flerov I N 2011 Specific heat, cell parameters, phase $T - p$ diagram, and permittivity of cryolite $(NH_4)_3Nb(O_2)_2F_4$ *Phys. Solid State* **53** 2147–53

[50] Fokina V D, Flerov I N, Gorev M V, Bogdanov E V, Bovina A F and Laptash N M 2007 Thermophysical studies of the phase transitions in $(NH_4)_3NbOF_6$ crystals *Phys. Solid State* **49** 1548–53

[51] Stern-Taulats E, Lloveras P, Barrio M, Defay E, Egilmez M, Planes A, Tamarit J-L, Mañosa L, Mathur N D and Moya X 2016 Inverse barocaloric effects in ferroelectric $BaTiO_3$ ceramics *APL Mater.* **4** 091102